

Electronic Supplementary Information:

Intratumoral H₂O₂-Triggered Release of CO from Metal Carbonyl-based Nanomedicine for Efficient CO Therapy

Zhaokui Jin^{†a}, Yanyuan Wen^{†a}, Liwei Xiong^b, Tian Yang^a, Penghe Zhao^a, Liwei Tan^c, Tianfu Wang^a, Zhiyong Qian^c, Bao-Lian Su^d, Qianjun He^{a*}

^a National-Regional Key Technology Engineering Laboratory for Medical Ultrasound, Guangdong Key Laboratory for Biomedical Measurements and Ultrasound Imaging, School of Biomedical Engineering, Shenzhen University, Shenzhen 518060, Guangdong, P. R. China

^b Hubei Key Laboratory of Plasma Chemistry and Advanced Materials, Wuhan Institute of Technology, Wuhan, 430073, P. R. China

^c State Key Laboratory of Biotherapy and Cancer Center, Collaborative Innovation Center for Biotherapy, West China Hospital, Sichuan University, Chengdu 610041, P. R. China

^d State Key Laboratory of Advanced Technology for Materials Synthesis and Processing, Wuhan University of Technology, Wuhan 430070, P. R. China.

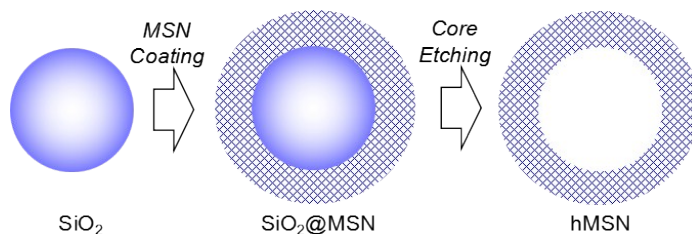
[†]These authors contributed equally to this work.

* corresponding author: nanoflower@126.com

Experimental Section

1. Synthesis and characterization of the advanced nano-carrier hollow mesoporous silica nanoparticle(hMSN)

The hMSN nano-carrier was synthesized by the combination of layer-by-layer coating and selective etching strategies, as demonstrated in the following Scheme S1.



Scheme S1.Schematic illustration for the layer-by-layer coating and selective etching strategy for

the synthesis of hMSN from SiO₂.

1.1 Preparation of the SiO₂ seed

The SiO₂ seeds were synthesized by a micro-emulsion method.^[1] In a typical procedure, the mixed solution of 60mL cyclohexane and 3mL Igepal CO@520 (NP-5) were sealed and stirred for 10min. Then, 420μL ammonia (30 wt%) was dropwise added and stirred for another 2 h. 600 μL tetraethyl orthosilicate (TEOS) was subsequently injected with a rate of 3 μL/min, and stirred for another 24 h at 20 °C. Finally, 10 mL absolute methanol(MeOH) was added to destroy the emulsion by 30 min stirring. The precipitate was collected by centrifugation and washed with ethanol (EtOH) twice to remove NP-5. The product was redispersed into 6 mL water.

1.2 Preparation of the core-shell nanostructure (SiO₂@MSN)

The SiO₂@MSN was constructed by a layer-by-layer coating method.^[1] Typically, 2 g cetyltrimethylammonium chloride solution (CTAC, 25 wt%) and 200 μL triethanolamine solution (TEAH, 10 wt%) were added into 11 mL H₂O in turn. After mixing completely, 2 mL above SiO₂ solution was added and sonicated for 10 min. The mixed solution was heated to 80 °C and stirred for at least 1 h until bubbles vanishing. Then, 220 μL TEOS were injected with a rate of 1 μL/min, and the solution kept stirring for another 12 h.

1.3 Synthesis of hMSN

The hMSN were synthesis using the structural difference-based selective etching strategy,^[1] as demonstrated in Scheme S1. Upon cooling to 50 °C, 10 mL above SiO₂@MSN solution was etched for 1 h with 954 mg Na₂CO₃. The precipitate was collected by centrifugation and washed with water and MeOH once in turn. The final product hMSN was achieved by the CTAC extraction with the MeOH solution of NaCl (1.5 wt%), washed with MeOH twice, and redispersed into dry MeOH.

1.4 Characterization of hMSN

The morphologies and meso-structures of the prepared SiO₂, SiO₂@MSN and hMSN were characterized by transmission electron microscopy (TEM, JEM-1200EX, 120 KV) and high resolution transmission electron microscopy (HRTEM, FEI Tecnai F20, 200 KV) equipped with EDS. As shown in Figure S2, SiO₂, SiO₂@MSN and hMSN all have high monodispersity and uniformity in size, and hMSN exhibits a clear hollow mesoporous structure with a particle size of about 120 nm. The pore structure and specific surface area of hMSN were measured by nitrogen absorption-desorption isotherms (N₂ adsorption, Micromeritics ASAP 2420). From Figure S3, it could be found that ...

2. Construction of the MnCO@hMSN nanomedicine

The loading of MnCO was using a facile nano-casting method. 8 mg MnCO was completely dissolved into 2 mL MeOH solution of hMSN (3.4 mg/mL) to get a pale yellow solution. The mixed solution was light-sealed and degassed under vacuum until the volume decreased to ~600 μL. Nanoparticles were collected by centrifugation and washed with MeOH once, and the supernatant/washing solutions were collected, metered to 10 mL, then diluted 20 times for the

measurement of drug loading capacity. The separated nanoparticles were further washed with H₂O twice and redispersed into H₂O (NOTICE: NO ULTRASOUND), obtaining a clear yellow solution (Figure S4).

The MnCO loading capacity of hMSN was detected by two different methods, the UV method and the EDS method, as following.

As to the UV method, several different concentrations of methanol solution of MnCO were firstly prepared and detected by UV spectrophotometer to get the absorption intensities at 340 nm, and then make a standard curve with them as shown in Figure S5A. The 340-nm absorbances of above-mentioned supernatant clear solutions of MnCO before and after loading with hMSN were measured and used to calculate the MnCO loading capacity with the standard curve according to the Beer-Lambert law, as shown in Figure S5B. The calculated loading capacity by the UV method is about 474 mg MnCO per gram silica.

As to the EDS method, when the element mapping was collected (Figure 2B), the molar ratio of Mn to Si was measured by EDS analysis to be 0.142. Therefore, the MnCO loading capacity of hMSN could be calculated to be 462 mg Mn₂(CO)₁₀ prodrug per gram hMSN. It can be found that the measured loading capacities by these two methods are close.

3. Characterization of the MnCO@hMSN nanomedicine

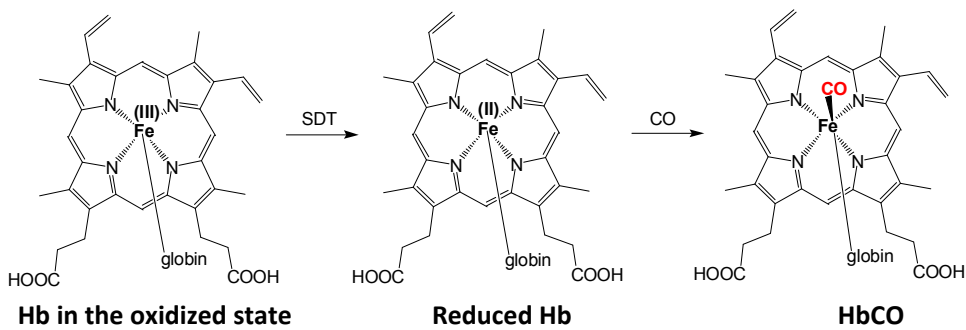
The morphology and structure of the constructed MnCO@hMSN were measured by TEM by the above-mentioned method. At the same time, the mapping of Si/O/C/Mn elements was collected for localization of the MnCO prodrug and the hMSN carrier. As shown in Figure 2B, some C signal distributes outside hMSN, which derives from the carbon supporting film on sample platform, while clearly cloudy C/Mn signals on hMSN suggests that MnCO indeed has been encapsulated into hMSN. The composition of MnCO@hMSN was characterized by attenuated total reflectance Fourier transform infrared spectroscopy (ATR-FTIR). Concentrated sample solutions were dropped on the universal diamond ATR sampling accessory and slowly dried by blowing with nitrogen gas. FT-IR spectra (Figure S5) were then collected on a Thermo-Nicolet Nexus 670 ATR-IR spectrometer.

4. The H₂O₂ responsiveness mechanism of MnCO for H₂O₂-triggered CO release

The H₂O₂ responsiveness mechanism of MnCO was evaluated by comparing the reactivity of MnCO in the phosphate buffer solutions (PBS) in the absence and presence of H₂O₂ by XRD characterization of reactants and products. The fresh crystal powder of MnCO was dispersed into two PBSs with and without H₂O₂ by gentle shaking. After statically settled for 24 h, products were collected and their composition were analyzed by powder X-ray diffraction using a M21X diffractometer (Cu K α , $\lambda=1.54056\text{ \AA}$) operated at 40 kV and 200 mA. The experimental diffraction patterns were collected with a step scanning range of 5°-80° at room temperature.

5. Measurement of CO release from the MnCO@hMSN nanomedicine in PBS by a

hemoglobin (Hb) method



Scheme S2. The Hb method for detecting the release of CO.^[2]

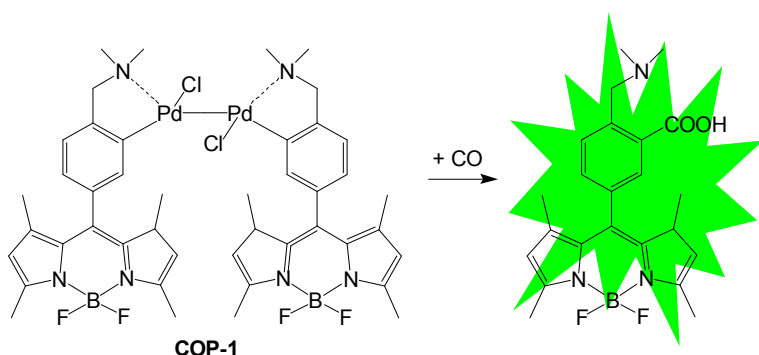
The released CO in PBS was detected spectrophotometrically by measuring the conversion of hemoglobin (Hb) to carboxyhemoglobin (HbCO), as demonstrated by Scheme S2. Firstly, hemoglobin from bovine erythrocytes (MP Biomedicals, 4.2 μM final concentration) was dissolved completely in phosphate buffered saline (10 mM, pH=7.4, PBS), and then was reduced by adding sodium dithionite (SDT, 1.6 mg) under a nitrogen atmosphere. An aqueous solution of MnCO@hMSN (200 μL) was deoxygenated by bubbling with nitrogen gas and then added into the above Hb solution. Immediately, the whole 4 mL reaction solution was sealed in a 4 mL UV quartz cuvette. The UV adsorption spectra of the solution (350–600 nm) were collected on a Genesys 10S UV-Vis spectrophotometer (Thermo Sci.), as shown in Figure S7. In order to eliminate influencing factors and enhance the accuracy, two strong adsorption bands at 410 nm and 430 nm, which were attributed to HbCO and Hb respectively, were used to quantify the conversion of Hb to HbCO (see Figure S7). The Beer-Lambert law was used to calculate the concentration of released CO (C_{CO}) according the following function(see Figure S8).^[2]

$$C_{CO} = \frac{528.6 \times I_{410nm} - 304 \times I_{430nm}}{216.5 \times I_{410nm} + 442.4 \times I_{430nm}} C_{Hb}$$

wherein, C_{CO} and C_{Hb} express the released CO concentration and the initial Hb concentration (4.2 μM), respectively. I_{410nm} and I_{430nm} express the intensities of collected spectrum at 410 nm and 430 nm, respectively.

6. Measurement of CO release from the MnCO@hMSN nanomedicine inPBS and cells using COP-1

Besides the Hb method, the COP-1 method was also employed to measure the CO release. Furthermore, the intracellular released CO was also detected by using the CO Probe 1 (COP-1). As indicated by Scheme S3, the product of COP-1 with CO generates a green fluorescence (475 nm excitation, 510 nm emission). COP-1 was synthesized according to the Chang's method.³



Scheme S3. The COP-1 method for detecting the release of CO.^[2]

AGS cells and 661W cells (5×10^4 cells/well) were paved in a 24-wellplate, respectively. After incubation for 12 h, the culture medium in each well was replaced with 1 mL fresh medium with 100 $\mu\text{g}/\text{mL}$ MnCO@hMSN nanomedicine. After 4h incubation, the medium was removed and replaced with 1 mL fresh medium containing COP-1 (1 $\mu\text{g}/\text{mL}$ in DMSO). After 10 min, cells were washed twice with PBS to remove residual COP-1 and nanoparticles. Then, the cells were observed under fluorescence microscopy to qualitatively measure the intracellular release of CO from the MnCO@hMSN nanomedicine(Figure S9). Meanwhile, a control with COP-1 and hMSN was also used to check the effect of the hMSN nano-carrier on the fluorescence of COP-1.

7. Cytotoxicity measurement of the MnCO-GO nanomedicine

The *in vitro* cytotoxicity of the MnCO@hMSN nanomedicine to cancer cells and normal cells was evaluated using five different cell lines (661W as a normal model cell line, 375, HepG2, HCT116 and AGS as the cancer model cell lines). Firstly, the intracellular H_2O_2 contents of every cell lines were analyzed with a hydrogen peroxide assay kit (Beyotime, China) according to the manufacturer instruction. Briefly, test tubes containing 50 μL test solutions were placed at room temperature for 30 min and measured immediately with a spectrometer at a wavelength of 560 nm. Absorbance values were calibrated to a standard curve generated with known concentrations of H_2O_2 .

Cells were seeded in a 96-well plate at a density of 1×10^4 cells/well, and were cultivated with a DMEM culture medium containing 10% fetal bovine serum at 37 °C in a humidified and 5% CO_2 incubator. After incubation for 24 h at 37 °C in 100 μL culture medium per well, the culture medium was discarded, and the cells were then treated with 100 μL DMEM solution of MnCO@hMSN at final concentrations of 6.25–100 $\mu\text{g}/\text{mL}$. After incubation for 24 h, 10 μL CCK-8 solution was added into each well. After incubation for another 1 h, the plate was read using a Bio-Tek multi-mode microplate reader (absorption wavelength 450 nm).The cytotoxicity was expressed as the percentage of cell viability as compared with the blank control(Figure S10 and Figure S11). Each data point was represented as a mean \pm standard deviation of eight independent experiments ($n = 8$).Meanwhile, the controls with hMSN and with raw MnCO were also used to check the cytotoxicity of the hMSN carrier and the hydrophobic MnCO prodrug against AGS cells and 661W cells, respectively.

8. Tumor model and *in vivo* therapy efficacy

The 4T1 tumor model was established in Balb/c-nu female mice by inoculating 1×10^7 MCF-7 cells into the forelimb of each nude mouse, and was used for evaluating *in vivo* therapy efficacy of the MnCO@hMSN nanomedicine. After the mean volume of the tumors reached approximately $\sim 500\text{mm}^3$, the tumor-bearing mice were randomly divided into 3 groups, then injected with the MnCO@hMSN nanomedicine (7.5mg/mL in PBS), the hMSN carrier (7.5mg/mL in PBS) and PBS as blank control (three-point injection, 20 μL /point), respectively. At given time points, tumor volume was measured by length \times width \times width $\times 0.5$. The mouse survival and body weight were also recorded. All animal experiments were approved by the Institutional Animal Care and Use Committee of Sichuan University (Chengdu, China) and were carried out in compliance with the approved guidelines (IACUC-S200904-P001). All the mice were treated humanely throughout the experimental period.

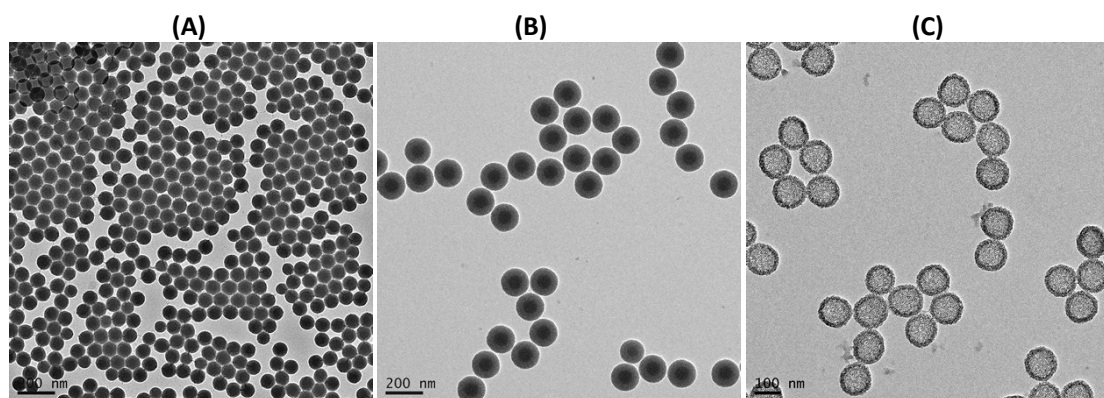


Figure S1. TEM images of SiO_2 seeds (A), $\text{SiO}_2@\text{MSN}$ (B), and hMSN (C).

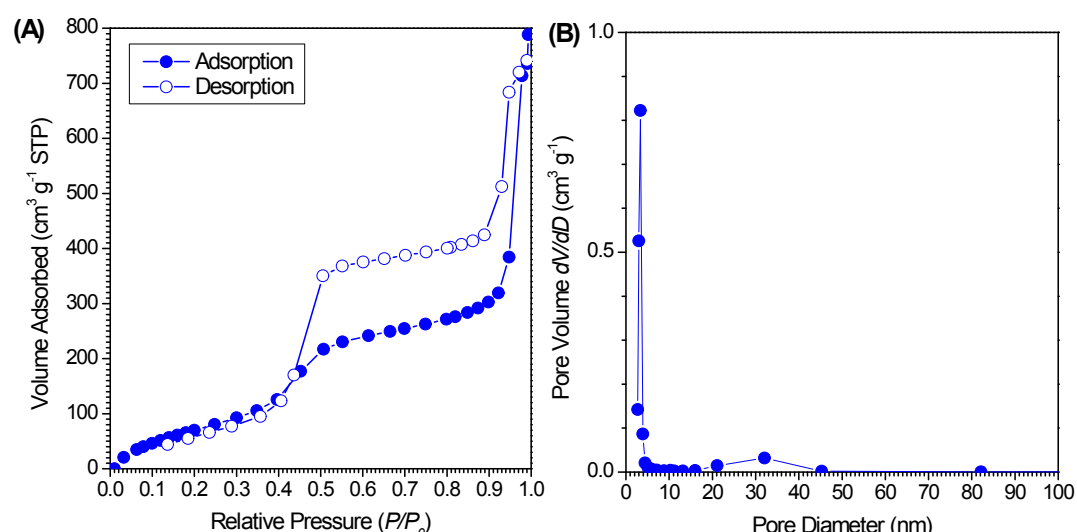


Figure S2. Nitrogen adsorption–desorption isotherm (A) and pore size distribution curve(B)of hMSN.

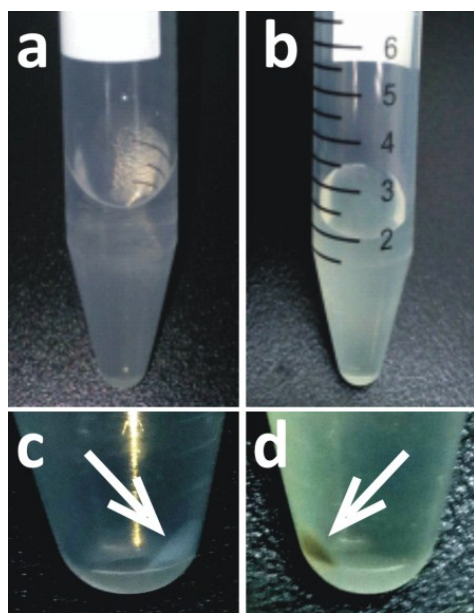


Figure S3. Typical digital photographs of the aqueous solutions of hMSN before (a,c) and after (b,d) MnCO loading, and collected particles before (c) and after (d) MnCO loading. Blue hMSN particles become yellow (as pointed by arrows in figures c and d), indicating the successful loading of MnCO. After loading of MnCO, MnCO@hMSN inherits excellent monodispersity of hMSN in water, as suggested by clear hMSN and MnCO@hMSN solutions in figures a and b.

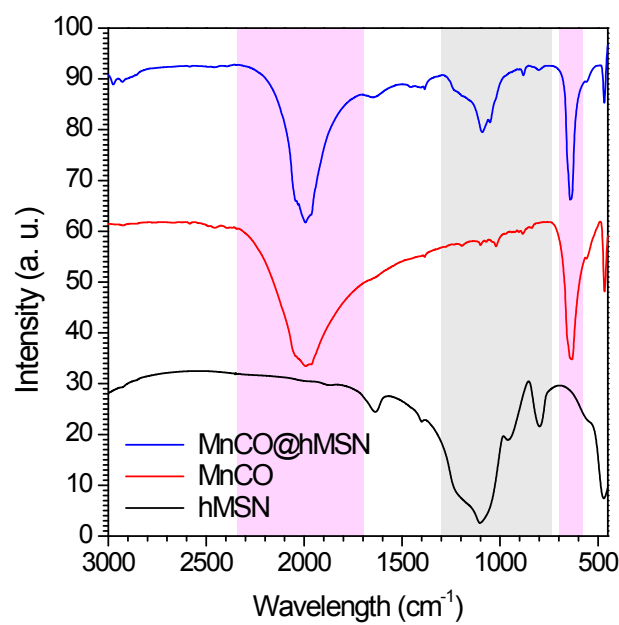


Figure S4. FT-IR spectra of the MnCO prodrug, the hMSN carrier, and the MnCO@hMSN nanomedicine.

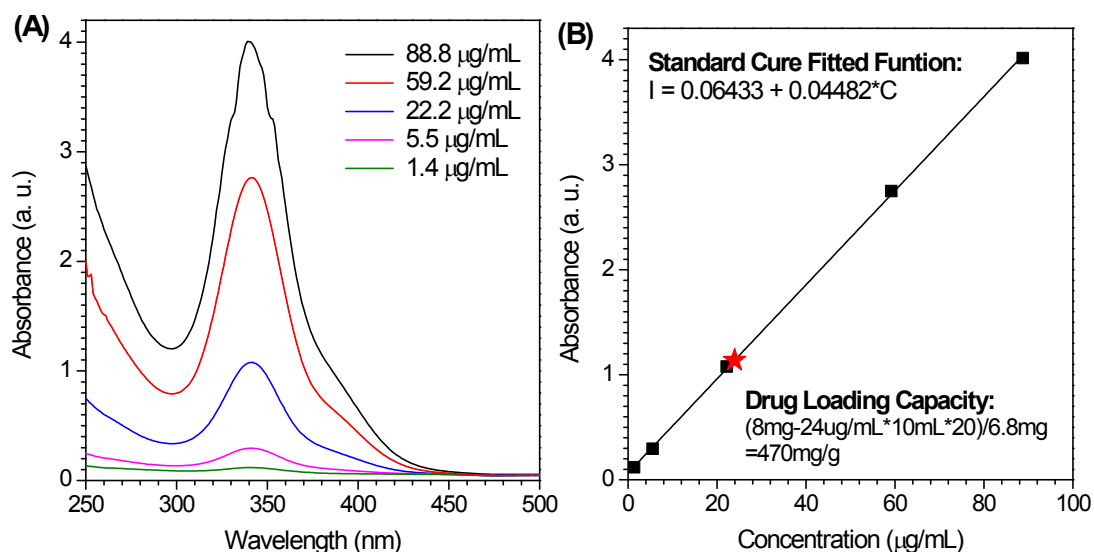


Figure S5. UV-vis absorption spectra of MnCO solutions (in MeOH) at different concentrations (A), and the fitted standard curve (B), by which the concentration of the supernatant solution after MnCO loading is calculated as shown by the red star symbol. Furthermore, the MnCO loading capacity of hMSN is calculated to be 474 mg MnCO per gram hMSN according to the difference of MnCO concentration between before and after loading, as indicated in figure B.

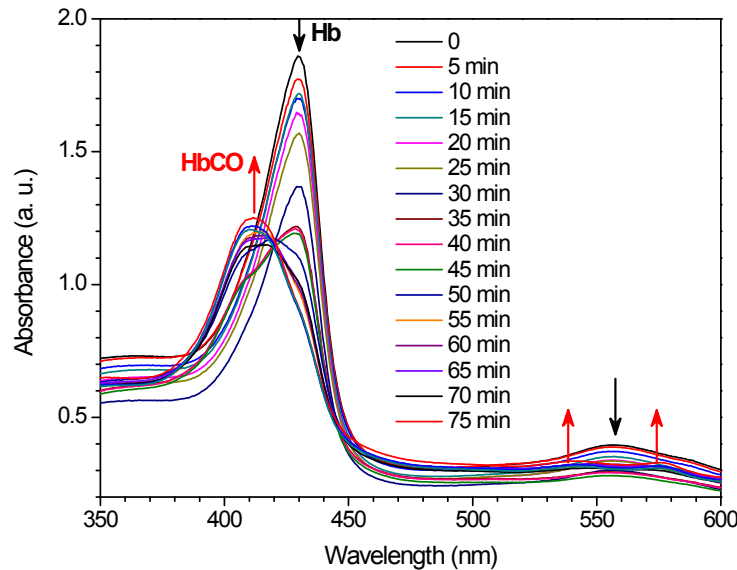


Figure S6. UV monitoring of the CO release process of the MnCO@hMSN nanomedicine in the PBS containing 32 µM H₂O₂ by the Hb method.

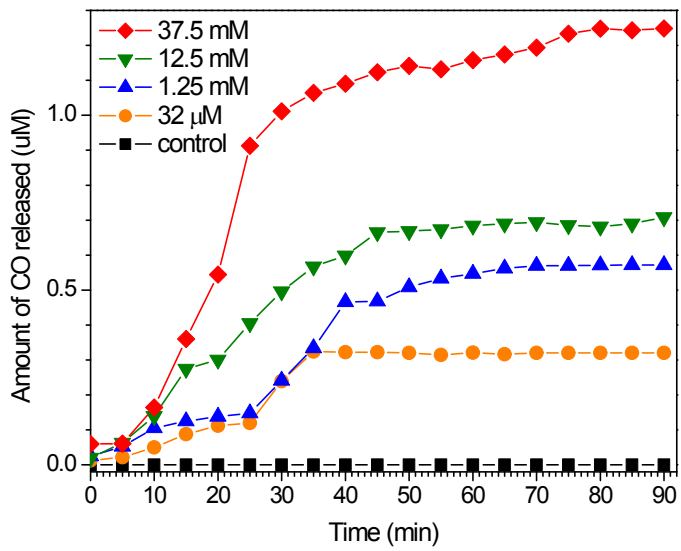


Figure S7. The responsiveness of MnCO@hMSN to different H₂O₂ concentrations for CO release, which was detected by the Hb method.

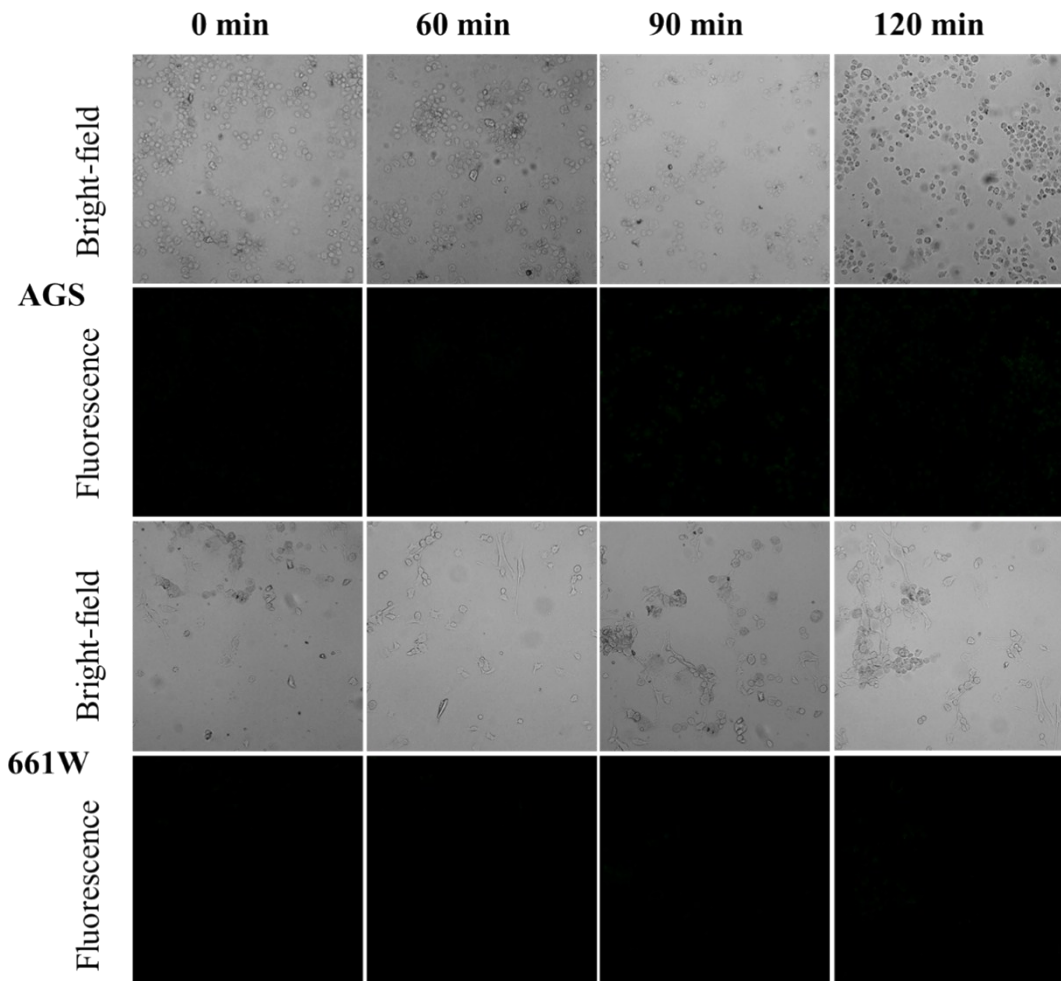


Figure S8. Bright field images and corresponding fluorescence images of AGS cells and 661W cells treated with the hMSN for different time periods in the presence of COP-1.

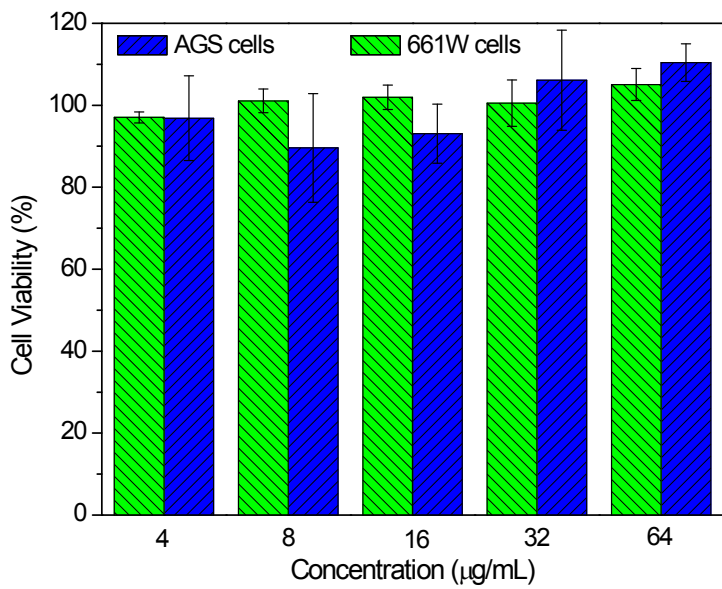


Figure S9.Cytotoxicities of the hMSN nanocarrier against AGS and 661 cells.

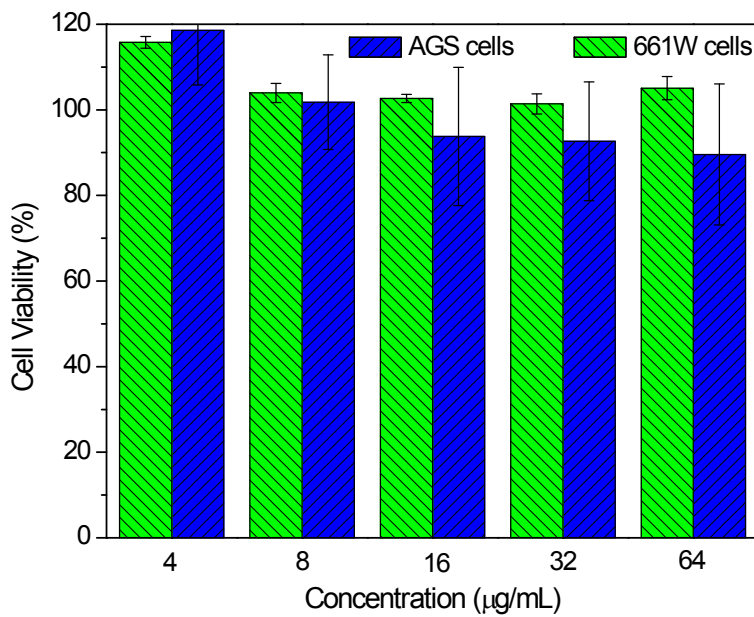


Figure S10.Cytotoxicities of the raw MnCO prodrug against AGS and 661 cells.

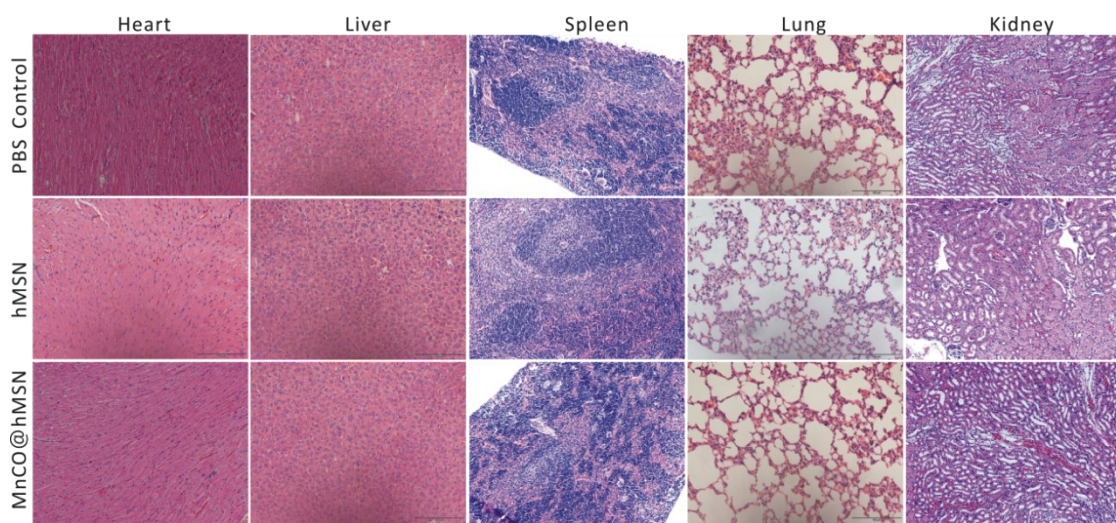


Figure S11. Histological examination of tissues (heart, liver, spleen, lung and kidney) from mice treated with the PBS control, the hMSN nano-carrier and the MnCO@hMSN nanomedicine (7.5 mg/mL in PBS) after 22 days by the hematoxylin–eosin staining method.

Reference

1. F. Chen, H. Hong, S. Shi, S. Goel, H. F. Valdovinos, R. Hernandez, C. P. Theuer, T. E. Barnhart, W. Cai, Engineering of hollow mesoporous silica nanoparticles for remarkably enhanced tumor active targeting efficacy, *Sci. Rep.* 2014, **4**, 5080–5080.
2. Q. He, D. O. Kiesewetter, Y. Qu, X. Fu, J. Fan, P. Huang, Y. Liu, G. Zhu, Y. Liu, Z. Qian, X. Chen, NIR-responsive on-demand release of CO from metal carbonyl-caged graphene oxide nanomedicine, *Adv. Mater.* 2015, **27**, 6741–6746.
3. B. W. Michel, A. R. Lippert, C. J. Chang, A reaction-based fluorescent probe for selective imaging of carbon monoxide in living cells using a palladium-mediated carbonylation, *J. Am. Chem. Soc.* 2012, **134**, 15668–15671.